Available online at www.sciencedirect.com
SCIENCE DIRECT®
International Journal of Heat and Fluid Flow 24 (2003) 389–398
International Journal of HEAT AND FLUID FLOW
www.elsevier.com/locate/ijhff

Numerical investigations of liquid–solid slurry flows in a fully developed turbulent flow region

J. Ling, P.V. Skudarnov, C.X. Lin, M.A. Ebadian *

Hemispheric Center for Environmental Technology, Center for Engineering and Applied Sciences, Florida International University, 10555 West Flagler Street, EAS-2100, Miami, FL 33174, USA

Received 6 December 2001; accepted 14 February 2003

Abstract

In this paper, a simplified 3D algebraic slip mixture (ASM) model is introduced to obtain the numerical solution in sand–water slurry flow. In order for the study to obtain the precise numerical solution in fully developed turbulent flow, the RNG K–ε turbulent model was used with the ASM model. An unstructured (block-structured) non-uniform grid was chosen to discretize the entire computational domain, and a control volume finite difference method was used to solve the governing equations. The mean pressure gradients from the numerical solutions were compared with the authors' experimental data and that in the open literature. The solutions were found to be in good agreement when the slurry mean velocity is higher than the corresponding critical deposition velocity. Moreover, the numerical investigations have displayed some important slurry flow characteristics, such as volume fraction distributions, slurry density, slip velocity magnitude, slurry mean velocity distributions, and slurry mean skin friction coefficient distributions in a fully developed section, that have never been displayed in the experiments.

Keywords: Granular flow; Multiphase flow; Numerical analysis; Slurries; Turbulence

1. Introduction

Slurry pipeline transportation is a popular mode of transportation in various industries. It has several advantages, such as its friendliness to the environment and its relatively low operation and maintenance costs. In general, slurry transportation is divided into three major flow patterns: (1) pseudo-homogeneous flow (or homogeneous flow) and heterogeneous flow; (2) heterogeneous and sliding bed flow (or moving bed flow), and (3) saltation and stationary bed flow (Doron and Barnea, 1996). Pseudo-homogeneous flow is a slurry flow pattern in which the slurry flows at a very high velocity and all solid particles are distributed nearly uniformly across the pipe cross-section. With a decrease in slurry flow rate, the heterogeneous flow pattern occurs when there is a concentration gradient in the direction perpendicular to the pipe axis, with more particles transported at the lower part of the pipe cross-section, as is the case in most practical applications. As the slurry flow rate is reduced further, the solid particles accumulate at the bottom of the pipe and form a moving bed layer, while the upper part of the pipe cross-section is still occupied by a heterogeneous mixture. When the slurry flow rate is too low to suspend all solid particles, a stationary bed layer at the bottom of the pipe cross-section is observed. This is the saltation and stationary bed flow (Vocaldo and Charles, 1972; Parzonka et al., 1981). The slurry velocity associated with the formation of a stationary bed layer is called the critical deposition velocity. A bed layer in the slurry pipeline is unstable and dangerous during the operation of pipeline transportation. It probably enhances pipe wear and causes plugging or blockage of the pipeline. As a result, it should be avoided in design and operation of the pipeline transportation system.

Slurry flow is very complex. In a survey of the open literature on slurry transportation investigations, it was found that most investigations were made in laboratories to determine pressure gradients and critical deposition velocities in slurry flows. Doron et al. (1987) and Doron and Barnea (1993) proposed two-layer and

* Corresponding author. Tel.: +1-305-348-3585; fax: +1-305-348-4176.
E-mail address: ebadian@hcet.fiu.edu (M.A. Ebadian).

0142-727X/03/$ - see front matter © 2003 Elsevier Science Inc. All rights reserved.
doi:10.1016/S0142-727X(03)00018-3

Nomenclature

$\vec{a}$	secondary phase particle's acceleration, m/s^2
$C_{1\varepsilon}$, $C_{2\varepsilon}$, C_μ	constants
d_p	solid particle diameter, m
E	empirical constant
F	body force, N/m^2
f_m	mean friction factor
g	acceleration of gravity, m/s^2
I	turbulent intensity level
K	turbulent kinetic energy, m^2/s^2
k_v	von Karman's constant
k_p	turbulent kinetic energy at point p, m^2/s^2
L	pipeline length, m
Pr_t	turbulent Prandtl number for energy
S	modulus of the mean rate-of-strain tensor
V	slurry mean velocity, m/s
u_m	mass-averaged velocity, m/s
u_{Dk}	drift velocity, m/s
u_p	mean velocity of the fluid at point p, m/s
$\vec{v}_{qp}$	slip velocity, m/s
y_p	distance from point p to the wall, m
$\Delta p/\Delta L$	mean pressure gradient of the slurry flow, Pa/m

Greeks

α_k	volume fraction of solids
β	coefficient of thermal expansion
ρ_m	mixture density, kg/m^3
ρ_s	solid particle density, kg/m^3
ρ_w	water density, kg/m^3
ε	dissipation rate of turbulent kinetic energy, m^2/s^3
μ_m	viscosity of the mixture, kg/m s
τ_{pq}	particulate relaxation time, s

Subscripts

i, j, k	general spatial indices
m	mixture
s, z, w	silica sand, zircon sand, and water

three-layer models of the slurry flow, and Wilson and Pugh (1988) put forward a dispersive-force modeling in heterogeneous slurry flow, but these models were derived based on single-species slurry flow and cannot determine the slurry density and volume fraction distributions and the slip velocity between the liquid and solid particles. Nassehi and Khan (1992) provided a numerical method for the determination of slip characteristics between the layers of a two-layer slurry flow, but no comparisons of experimental results and numerical solutions were reported. In this paper, a simplified two-phase flow algebraic slip mixture (ASM) model (Manninen et al., 1996) is introduced to obtain the numerical solution in the sand–water slurry flow. A control volume finite difference method (CVFDM) is used to solve the governing equations, and an unstructured (block-structured) non-uniform grid is chosen to discretize the entire computational domain. The numerical investigations have displayed some important liquid–solid slurry flow characteristics, such as volume fraction distributions, slurry density, slip velocity magnitude, slurry mean velocity distributions, and slurry mean skin friction coefficient distributions in a fully developed section, that have never been displayed in the experiments.

2. Calculation models

2.1. Governing equations

The ASM model can model two-phase flow (fluid or particulate) by solving the momentum equation and continuity equation for the mixture, the volume fraction equation for the secondary phase, and an algebraic expression for the relative (slip) velocity. ASM assumes that a local equilibrium between the phases is reached over short spatial length scales. This assumption requires the dispersed phase (particles) accelerate rapidly to the terminal velocity (Manninen et al., 1996). Thus, typical dimension of the system should be much longer than the characteristic length scale of acceleration. The characteristic length scale of acceleration in water of a particle with a diameter of 1×10^{-4} m and density of 3300 kg/m^3 is on the order of 5×10^{-5} m (Manninen et al., 1996). This characteristic length is several orders of magnitude smaller than dimensions of the system we are modeling (see Section 3.1 for details); thus, ASM model assumptions are fully justified.

The continuity equation for the mixture in the ASM model is

$$\frac{\partial}{\partial t}(\rho_m)+\frac{\partial}{\partial x_i}(\rho_m u_{m,i})=0 \tag{1}$$

The momentum equation for the mixture can be expressed as

$$\begin{aligned}\frac{\partial}{\partial t}\rho_m u_{m,j}+\frac{\partial}{\partial x_i}\rho_m u_{m,i}u_{m,j}&=-\frac{\partial p}{\partial x_j}+\frac{\partial}{\partial x_i}\mu_m\left(\frac{\partial u_{m,i}}{\partial x_j}+\frac{\partial u_{m,j}}{\partial x_i}\right)\\&\quad+\rho_m g_i+F_j+\frac{\partial}{\partial x_i}\sum_{k=1}^{n}\alpha_k\rho_k u_{Dk,i}u_{Dk,j}\end{aligned} \tag{2}$$

where n is the number of phases, F is the body force, α_k is the volume fraction of solids, ρ_m is the mixture den-

sity, and μ_m is the viscosity of the mixture, which are expressed as

$$\rho_m = \sum_{k=1}^{n} \alpha_k \rho_k \text{ and } \mu_m = \sum_{k=1}^{n} \alpha_k \mu_k \tag{3}$$

$\vec{u}_m$ and $\vec{u}_{Dk}$ are mass-averaged velocity and drift velocities, which are expressed as

$$\vec{u}_m = \frac{\sum_{k=1}^{n} \alpha_k \rho_k \vec{u}_k}{\rho_m} \text{ and } \vec{u}_{Dk} = \vec{u}_k - \vec{u}_m \tag{4}$$

The slip velocity is defined as the velocity of the secondary phase (p) relative to the primary phase (q) velocity:

$$\vec{v}_{qp} = \vec{u}_p - \vec{u}_q \tag{5}$$

The drift velocity and slip velocity are connected by the following expression:

$$\vec{u}_{Dp} = \vec{v}_{qp} - \sum_{i=1}^{n} \frac{\alpha_i \rho_i}{\rho_m} \vec{v}_{qi} \tag{6}$$

The basic assumption in the ASM model is that, to prescribe an algebraic relation for the relative velocity, a local equilibrium between the phases should be reached over short spatial length scales. The form of the slip velocity is

$$\vec{v}_{qp} = \frac{(\rho_m - \rho_p) d_p^2}{18 \mu_q f_{drag}} \left(\vec{g} - \frac{\partial \vec{u}_m}{\partial t} \right) \tag{7}$$

where

$$f_{drag} = \begin{cases} 1 + 0.15\ Re^{0.687} & Re \leqslant 1000 \\ 0.0183\ Re & Re > 1000 \end{cases}$$

The volume fraction equation for the secondary phase is

$$\frac{\partial}{\partial t}(\alpha_p \rho_p) + \frac{\partial}{\partial x_i}(\alpha_p \rho_p u_{m,i}) = -\frac{\partial}{\partial x_i}(\alpha_p \rho_p u_{Dp,i}) \tag{8}$$

This ASM model can be applied in the laminar and turbulent two-phase flows. In practice, since slurry transportation is in the fully developed turbulent flow, the RNG K–ε turbulent model is used with the ASM model in this study. The turbulent kinetic energy in RNG K–ε turbulent model is

$$\frac{\partial}{\partial t}(\rho_m k) + \frac{\partial}{\partial x_i}(\rho_m u_{m,i} k) = \frac{\partial}{\partial x_i}\left[\left(a_k \mu_m \frac{\partial k}{\partial x_i} \right) \right] + \mu_t S^2 - \rho_m \varepsilon \tag{9}$$

Dissipation rate of the turbulent kinetic energy is

$$\frac{\partial}{\partial t}(\rho_m \varepsilon) + \frac{\partial}{\partial x_i}(\rho_m u_{m,i} \varepsilon) = \frac{\partial}{\partial x_i}\left[\left(a_\varepsilon \mu_m \frac{\partial \varepsilon}{\partial x_i} \right) \right] + C_{1\varepsilon} \frac{\varepsilon}{k} \mu_t S^2 - C_{2\varepsilon} \rho_m \frac{\varepsilon^2}{k} - R \tag{10}$$

where the coefficients a_k and a_ε are the inverse effect Prandtl numbers for k and ε, respectively. In the high-Reynolds-number limit, $a_k = a_\varepsilon \cong 1.393$. $C_{1\varepsilon}$ and $C_{2\varepsilon}$ are equal to 1.42 and 1.68. β and Pr_t are the coefficient of thermal expansion and the turbulent Prandtl number for energy. S is the modulus of the mean rate-of-strain tensor, S_{ij}, which is defined as

$$S = \sqrt{2 S_{ij} S_{ij}} \quad \text{and} \quad S_{ij} = \frac{1}{2}\left(\frac{\partial u_i}{\partial x_j} + \frac{\partial u_j}{\partial x_i} \right) \tag{11}$$

R in Eq. (10) was expressed as

$$R = \frac{C_\mu \rho_m \eta^3 (1 - \eta/\eta_0)}{1 + \zeta \eta^3} \cdot \frac{\varepsilon^2}{k} \tag{12}$$

where $\eta = S \cdot k/\varepsilon$, $\eta_0 \approx 4.38$, $\zeta = 0.012$, and $C_\mu = 0.085$.

2.2. Boundary conditions

Non-slip boundary condition is imposed on the walls, and heat transfer is not considered in the entire computational domain. For this paper, in the near-wall zone, the standard wall function proposed by Launder and Spalding (1974) was chosen due to its wide application in industrial flows. When the mesh is such that $y^* \leqslant 11.225$ at the wall-adjacent cells, the viscous force is dominant in the sublayer. The laminar stress–strain relationship can be applied:

$$u^* = y^* \tag{13}$$

$$y^* = \frac{\rho_m C_\mu^{1/4} k_p^{1/2} y_p}{\mu_m} \tag{14}$$

The logarithmic law for the mean velocity is known to be valid for $y^* \succ 11.225$ (Fluent Inc., 1996). It can be expressed as

$$u^* = \frac{1}{k} \ln(E y^*) \tag{15}$$

where k is von Karman's constant, C_μ is turbulent model constant, and k_p and y_p are the turbulent kinetic energy at point p and distance from point p to the wall, respectively.

To simplify the simulations, the mean velocity inlet boundary condition and pressure outlet boundary condition are imposed on the inlet and outlet of slurry pipeline:

$$u_{x,\text{inlet}} = \text{constant},\ u_{y,\text{inlet}} = u_{z,\text{inlet}} = 0,\ \text{and}$$
$$p_{\text{outlet}} = \text{constant} \tag{16}$$

3. Numerical computation

3.1. Physical problems and grid system

The geometry and physical problem studied in this paper are as follows:

Horizontally straight pipeline length, $L = 1.4$ m; inner diameter of the pipe, $d = 0.0221$ m; range of the volume

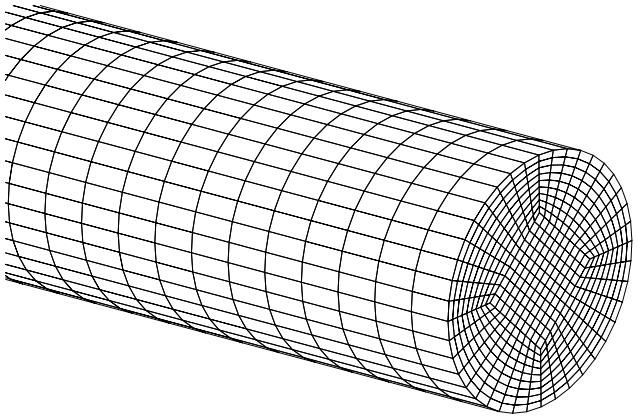

Fig. 1. Unstructured grid of the horizontal pipeline.

fraction of solid, α_k, is 10–20%; range of mean velocity of the slurry flow is 1–3 m/s; the densities of silica sand and zircon sand are 2380 and 4223 kg/m^3; mean particle diameter, d_p, is 1.1×10^{-4} m.

The length of the computational domain, $x/d \geqslant 50$, was based on the suggestions from Wasp et al. (1979) and Brown and Heywood (1991) to ensure that fully developed flow results could be obtained in the pipeline computational domain. A multi-block unstructured non-uniform grid system with hexahedral elements was used to discretize the computational domain, as shown in Fig. 1. This unstructured grid system has five blocks to form the entire computational pipeline. The distribution of the grid on the circumference of computational pipeline is uniform, and each hexahedral element in the grid system contains 27 nodes. The grid independent study was made to select the optimum grid distribution in this investigation, as shown in Table 1. From Table 1, V was mean velocity of the slurry flow, and $\Delta p/\Delta L$ and f_m were mean pressure gradient of the slurry flow and mean friction factor in fully developed turbulent flow, respectively. f_m could be obtained from

$$f_m = \frac{1}{2\pi}\int_0^{2\pi} f_\theta \mathrm{d}\theta \tag{17}$$

where

$$f_\theta = \frac{\tau_w}{\frac{1}{2}\rho_m V_m^2}$$

The grid distribution, 460×400, shown in Table 1 could ensure a satisfactory solution for the slurry flow.

3.2. Numerical method

In the numerical investigation of slurry transportation, all governing equations, wall boundary conditions, and inlet and outlet boundary conditions were solved in a Cartesian coordinate system by the CFD solver, FLUENT 5, which used a CVFDM. Heat transfer was neglected, and the slurry flows were steady state. At the same time, the slurry flows were in pseudo-homogeneous flow (or homogeneous flow), and heterogeneous flow and sliding bed flow (or moving bed flow). The second-order upwind scheme was selected as the discretization scheme in the governing equations. The SIMPLE algorithm from Dormaal and Raithby (1984) was used to resolve the coupling between the velocity and the pressure. To avoid the divergence, the under-relaxation technique was applied in all dependent variables. In the investigation, the under-relation factor for the pressure, p, was 0.2 and 0.3, that for the velocity components was 0.5–0.7, and those for the turbulence kinetic energy and turbulence dissipation rate were 0.6–0.8. The segregated solver was adopted to solve the governing equations sequentially. In the segregated solution method, each discrete governing equation was linearized implicitly with respect to that equation's dependent variable. A point implicit (Gauss-Seidel) linear equation solver was used in conjunction with an algebraic multi-grid method to solve the resultant scalar system of equations for the dependent variable in each cell. The numerical computation was considered converged when the residual summed over all the computational nodes at nth iteration, R_ϕ^n, satisfied the following criterion:

$$\frac{R_\phi^n}{R_\phi^m} \leqslant 10^{-4} \tag{18}$$

where R_ϕ^m is the maximum residual value of ϕ variable after m iterations.

All the numerical computations in this paper were based on the grid distribution, 460×400, and carried out in an SGI Origin 2000 at the Hemispheric Center for Environmental Technology (HCET) at Florida International University (FIU) in Miami.

Table 1
Grid independent test ($V = 2$ m/s, $57 \leqslant x/d \leqslant 61$, $\alpha_k = 0.189$, $d_p = 0.00011$ m, silica sand–water slurry flow)

Cross-sectional × axial	224 × 300	340 × 300	460 × 300	500 × 300	460 × 400	460 × 500
Total cells	67,200	108,000	138,000	150,000	184,000	230,000
$\Delta p/\Delta L$ (Pa/m)	2220	2205	2184	2177	2094	2154
f_m	2.53	2.463	2.325	2.325	2.335	2.335

4. Results and discussion

4.1. Comparisons of numerical and experimental data

The slurry mean pressure gradient is an important parameter in slurry transportation and pipeline design. To verify and check the numerical results from the ASM model, a lab-scale flow loop was constructed at HCET, and extensive experiments for the silica sand–water and zircon sand–water slurry flows were made (Skudarnov et al., 2001). Experimental data from Skudarnov et al. (2001) and other experimental data from Newitt et al. (1955) are compared with the numerical results, as shown in Fig. 2.

Fig. 2(a) shows the comparison of the numerical results with the experimental data from Skudarnov et al. and Newitt et al. in silica sand–water slurry flow with the same pipeline geometry, mean velocity, volume fraction, particle size, and particle density. Fig. 2(b) illustrates the comparison of the numerical results with the experimental data from Skudarnov et al. in zircon sand–water slurry flow. Based on the experimental investigations made by Skudarnov et al., the critical deposition velocities shown in Fig. 2(a) and (b) are 0.97 and 1.58 m/s, respectively.

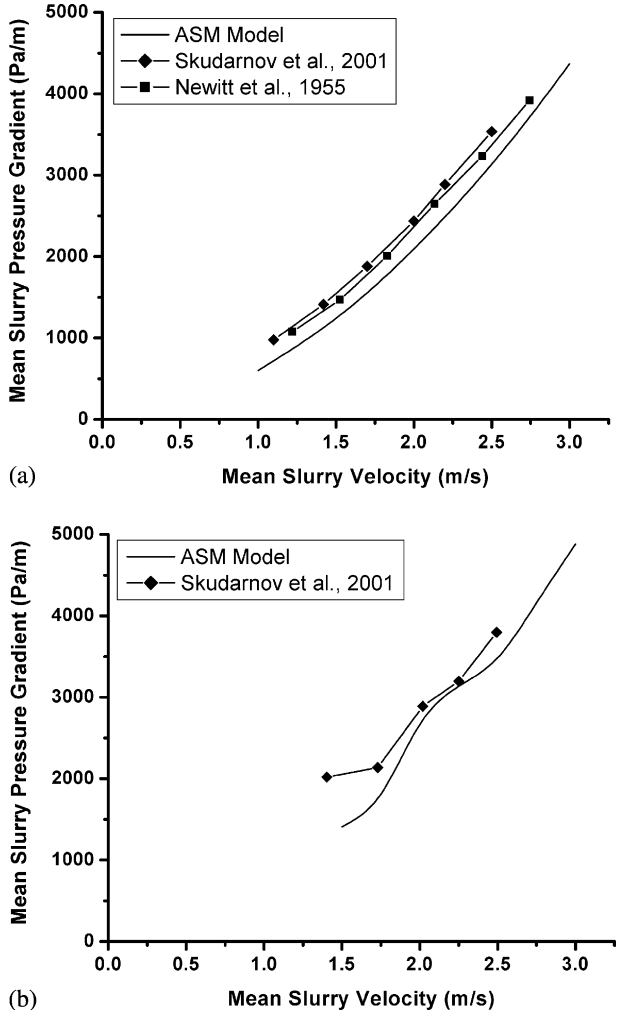

Fig. 2. Comparisons of the numerical solutions from ASM model with the experimental data from Skudarnov et al. (2001) and Newitt et al. (1955) in fully developed turbulent flow ($\rho_w = 998.2$ kg/m^3, $d = 0.0221$ m, $d_p = 0.000097$–0.00011 m). (a) Silica sand–water slurry, $\rho_s = 2381$ kg/m, $\alpha_k = 20\%$, (b) zircon sand–water slurry, $\rho_z = 4223$ kg/m, $\alpha_k = 10\%$.

It is clear that in Fig. 2(a) all slurry mean velocities for numerical results and experimental data are higher than the critical deposition velocity, and the numerical results are in good agreement with the experimental data although the numerical results from the ASM model result in a little under-prediction. From Fig. 2(b), the numerical results are still in good agreement with the experimental data, and a little under-prediction from the numerical results exists when the mean velocities of the zircon sand–water slurry flow in the numerical and experimental investigations are higher than the critical deposition velocity. A big discrepancy between the numerical results and experimental data takes place when the mean velocities of slurry flow in the numerical and experimental investigations are lower than corresponding critical deposition velocities, and the discrepancy would be further increased with a decrease in the slurry mean velocity.

In practice, the available flow area in the pipeline would be reduced, friction loss would be increased, and the pressure gradient in the slurry flow would be increased if the slurry velocity is lower than the corresponding critical deposition velocity and a stationary bed of the solids is formed in the experiments. However, the ASM model cannot change its available flow area when the slurry flow velocity is lower than the corresponding critical deposition velocity. As a result, a big discrepancy would occur for a slurry velocity that is lower than the critical deposition velocity. It is evident that the ASM model can provide a better prediction of pressure gradient if the slurry mean velocity is higher than the critical deposition velocity. Yet the ASM model would result in a bigger deviation if the slurry mean velocity is lower than the critical deposition velocity.

4.2. Slurry density, volume fraction, and skin friction factors

The slurry density and volume fraction are important parameters in slurry flow analysis. In experiments, it is difficult to measure the slurry density and volume fractions at any point of the pipe cross-sectional area, but it is easy to obtain them in numerical investigation.

The density distributions of the silica sand–water slurry flow with different mean velocities are shown in Fig. 3. Fig. 3(a) and (b) show the density distribution contours in the cross-sectional area of the pipeline in $V = 2$ and 3 m/s, and Fig. 3(c) illustrates the density

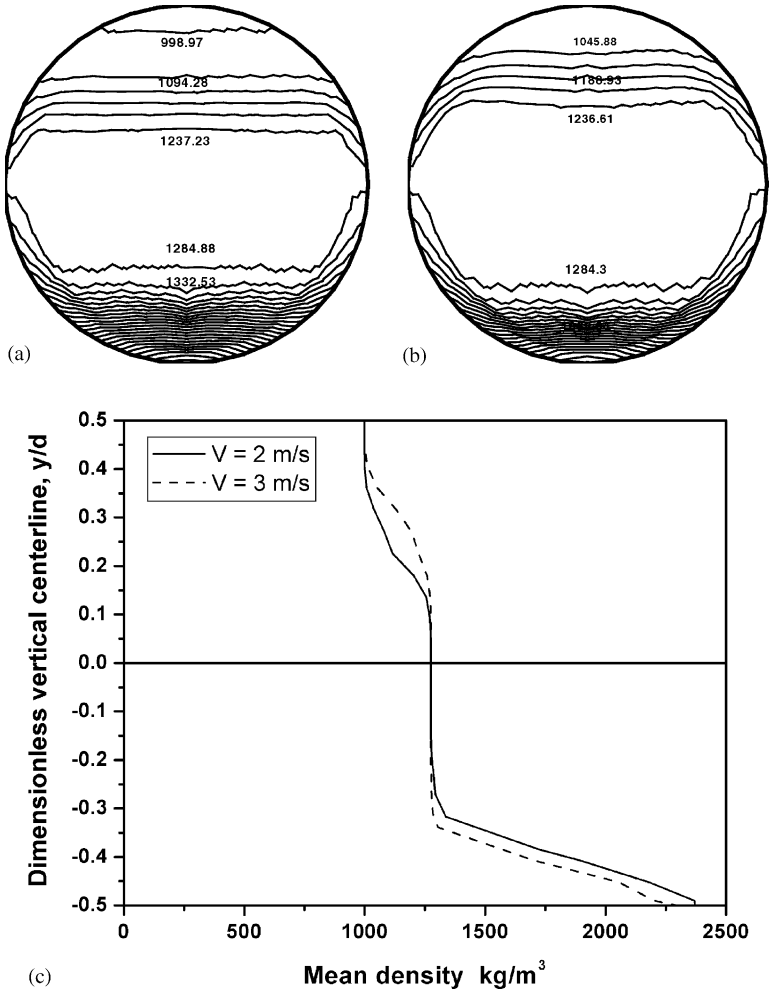

Fig. 3. Mean density distribution of the silica sand–water slurry flow ($\rho_s = 2381$ kg/m^3, $\rho_w = 998.2$ kg/m^3, $\alpha_k = 20\%$, $d = 0.0221$ m, $d_p = 0.00011$ m). (a) Density contours at $V = 2$ m/s, (b) density contours at $V = 3$ m/s and (c) density distribution along the vertical centerline.

distributions along the vertical centerline of the pipeline. It is clear from Fig. 3(a) and (b) that the density distribution contours are symmetrical in the horizontal direction. Because of the effect of the gravitational force, the density distribution contours are asymmetrical in the vertical direction. Since the density of solids is usually higher than that of primary fluid in slurry flows, on the top of the pipeline, the slurry mean density is relatively small and close to the water density, 998.2 kg/m^3, and in the lower part of the pipeline, the slurry mean density is increased gradually based on the action of gravity. In the central part of the pipeline, the slurry mean density is kept in a small variant range, which is about 1237–1284 kg/m^3, as shown in Fig. 3. However, it should be pointed out that the central area of the slurry flow with the small variance of the slurry mean density would be enlarged with an increase in the slurry mean velocity. For the same silica sand–water slurry flow with $\rho_s = 2381$ kg/m^3, $\rho_w = 998.2$ kg/m^3, $\alpha_k = 20\%$, $d = 0.0221$ m, and $d_p = 0.00011$ m, the central area with the slurry mean density in $V = 3$ m/s is bigger than that in $V = 2$ m/s, comparing Fig. 3(a) with (b).

Fig. 4 shows the volume fraction distribution contours of silica sand and water in the slurry flow with $V = 2$ and 3 m/s, $\alpha_k = 20\%$, $\rho_s = 2381$ kg/m^3, $\rho_w = 998$ kg/m^3, $d = 0.0221$ m, and $d_p = 0.00011$ m. Fig. 4 shows that the volume fractions of silica sand and water are symmetrical in the horizontal direction, but the volume fractions of silica sand and water have a big gradient in the vertical direction because of the asymmetry of density distribution in the slurry flows.

On top of the pipeline, the volume fraction of silica sand is close to zero, and the volume fraction of water approaches unity, as shown in Fig. 4. It means that most slurry flow on top of the pipeline is water. In the central part of the pipeline, the volume fractions of silica sand and water are almost kept in a small variant range. In the lower part of the pipeline, the volume fractions of silica sand are increased gradually, and the volume fractions of water are decreased accordingly. The sum of

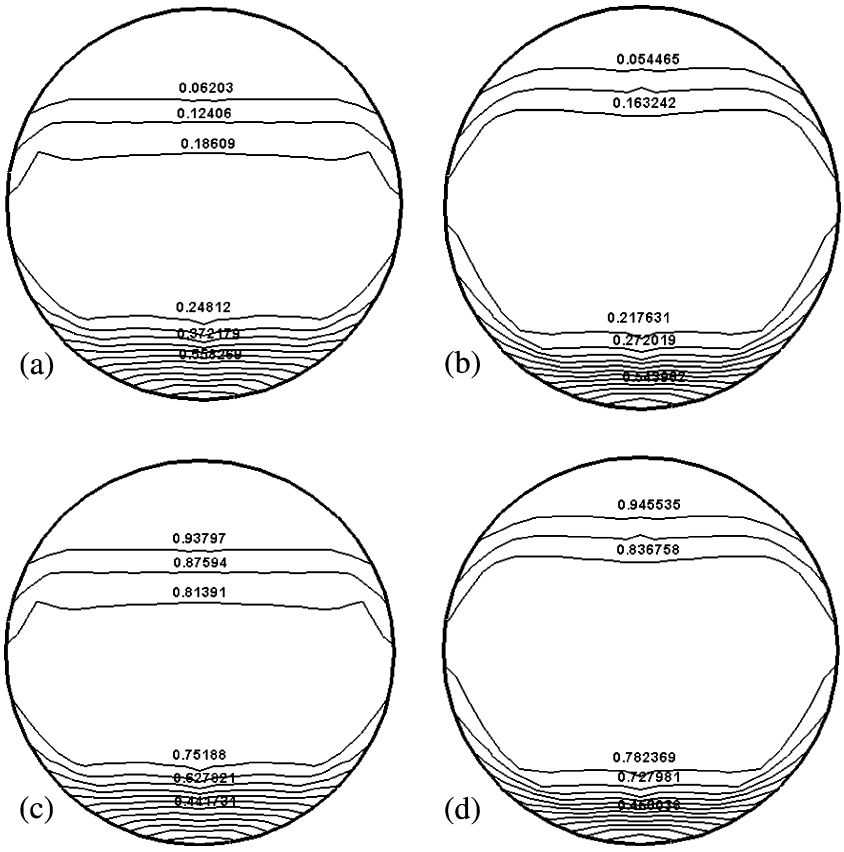

Fig. 4. Volume fraction contours of silica sand and water ($\rho_s = 2381$ kg/m^3, $\rho_w = 998.2$ kg/m^3, $\alpha_k = 20\%$, $d = 0.0221$ m, $d_p = 0.00011$ m). (a) Silica sand, $V = 2$ m/s, (b) silica sand, $V = 3$ m/s, (c) water, $V = 2$ m/s and (d) water, $V = 3$ m/s.

volume fractions of silica sand and water is equal to unity at any point of pipe cross-sectional area for the same slurry flow.

The slurry mean skin friction factors from the pipeline inlet to fully developed turbulent flow region are shown in Fig. 5. All slurry mean skin friction factors would drop sharply from the pipeline inlet, then, be raised gradually. At $x/d \geqslant 50$, the slurry mean skin friction factors are constant. Fig. 5 illustrates that the slurry mean skin friction factor would be constant in the fully developed turbulent flow. At the same time, Fig. 5 shows that the slurry mean skin friction factors will be increased as the slurry mean velocity and solid particle density increase. It means that a higher slurry mean velocity and solid particle density would result in a bigger flow loss and slurry mean pressure gradient in slurry pipeline transportation.

4.3. Slurry mean velocity profiles and slip velocity magnitude

The velocity profile of the slurry flow in the horizontal pipeline is mainly affected by the slurry density, volume fraction, and mean velocity. As a result, the velocity profile of the slurry flow in the cross-sectional area of the pipeline is a little bit different from that of single-phase flow. In general, the velocity profile in single-phase flow is symmetric around the pipe centerline, and liquid density is kept as a constant in the cross-sectional area of the pipeline. However, in the slurry flow, the velocity profile is asymmetrical around the pipe centerline.

Fig. 6 shows the mean velocity contours of silica sand–water and zircon sand–water slurry flows with $V = 3$ m/s, $\alpha_k = 20\%$, silica sand density $\rho_s = 2381$ kg/m^3, zircon sand density $\rho_z = 4223$ kg/m^3, water density $\rho_w = 998$ kg/m^3, $d = 0.0221$ m, and $d_p = 0.00011$ m. From Fig. 6, it is clear that the slurry mean velocities near the wall drop down sharply due to the strong viscous shear stress in the turbulent boundary layer and non-slip boundary condition on the wall. Like the slurry densities and volume fractions, the velocity distributions in the slurry flows are symmetrical in the horizontal direction, and the velocity profiles are asymmetric in the vertical direction due to the density gradients in the slurry flow.

It is clear from Fig. 6(a) and (b) that the maximum slurry velocity center appears at the upper part of the pipeline, not at the centerline. This phenomenon of slurry flow has been proved with experiments (Roco and

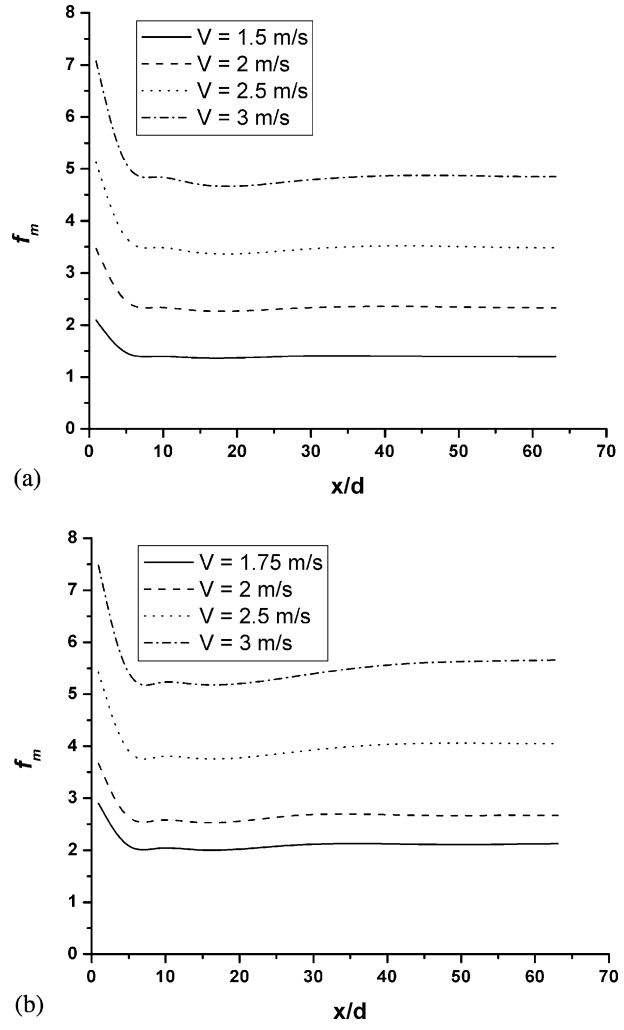

Fig. 5. Slurry mean skin friction factor distributions from the entrance to fully developed turbulent flow region ($d = 0.0221$ m, $d_p = 0.00011$ m). (a) Silica sand–water slurry, $\rho_s = 2381$ kg/m^3, $\alpha_k = 20\%$, (b) zircon sand–water slurry, $\rho_z = 4223$ kg/m^3, $\alpha_k = 10\%$.

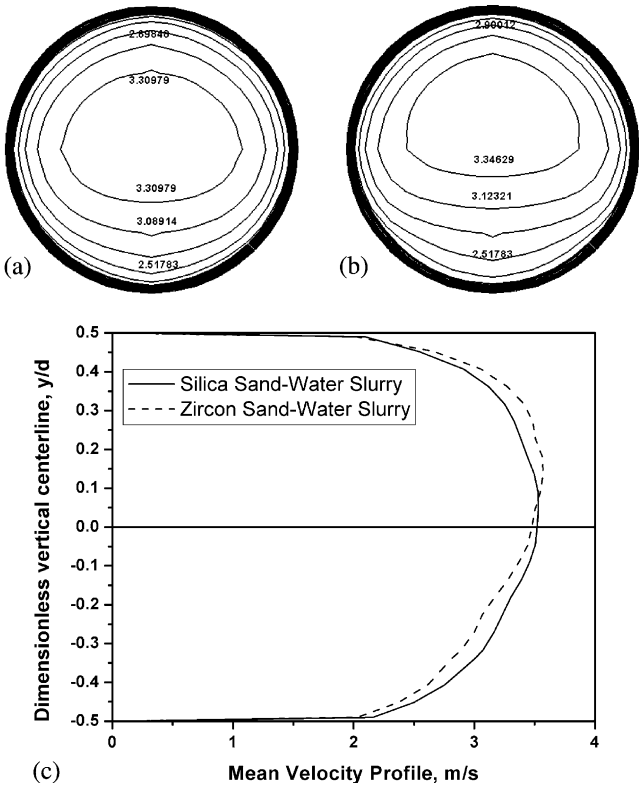

Fig. 6. Velocity contours and profiles of the silica sand–water and zircon sand–water slurry flows ($\alpha_k = 20\%$, $\rho_s = 2381$ kg/m^3, $\rho_z = 4223$ kg/m^3, $\rho_w = 988.2$ kg/m^3, $V = 3$ m/s, $d_p = 0.00011$ m, $d = 0.0221$ m). (a) Velocity isograms of silica sand–water, (b) velocity isograms of zircon sand–water and (c) velocity profiles along the vertical centerline.

Shook, 1985). On the other hand, comparing Fig. 6(a) with (b), it can be found that the location of the maximum velocity center in zircon sand–water slurry is higher than that in the silica sand–water when the slurry velocities, volume fractions, pipeline geometries, and particle diameters are the same. The figures indicate that the location of maximum velocity center with a higher slurry density is higher than that with a lower slurry density.

Fig. 6(c) shows the velocity profiles of the silica sand–water and zircon sand–water slurry flows with same velocities and geometries along the vertical centerline of the pipeline. Two slurry velocity profiles are asymmetric in the vertical direction, and the velocity profiles in the lower part of the pipe centerline would be lower than those in the upper part. This occurs because the density of solid particles is usually higher than that of liquid; the slurry density in the lower part of pipe centerline should be higher than those in the upper part based on the effect of gravity. As a result, compared with the upper part of the pipe centerline, water will spend more energy to drive silica sand in the lower part, which results in a lower slurry velocity in this area.

On the other hand, with an increase in the slurry density, the velocity profile in the upper part of pipe centerline would be increased further and that in the lower part would be reduced accordingly, as shown in Fig. 6(c).

The slip velocity in an ASM model is defined as the difference between the liquid velocity and solid particle velocity and is a function of the density of the slurry flow. Fig. 7 shows the slip velocity magnitudes of the silica sand–water slurry flow along the horizontal and vertical centerlines based on a non-slip boundary condition on the wall. As in Fig. 7(a), the slip velocity magnitude distribution is symmetric along the horizontal centerline since the slurry density along the horizontal centerline is symmetric. However, it is evident from Fig. 7(b) that the slip velocity magnitude distribution is asymmetric along the vertical centerline. The slip velocity magnitude in the upper part of the pipeline is relatively larger than that in the other parts since the slurry density in the upper part is relatively smaller. In

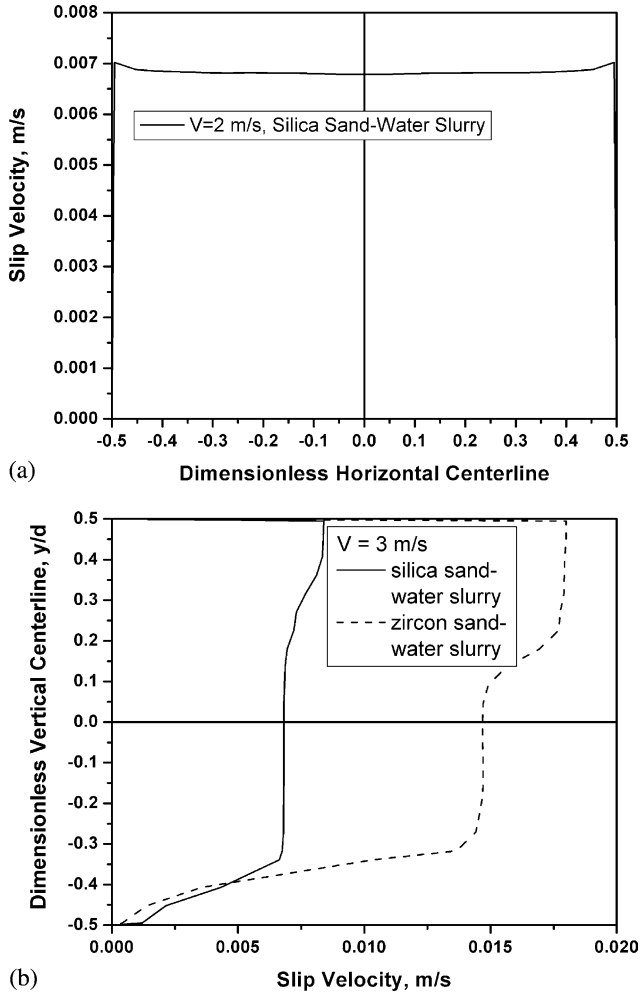

Fig. 7. Slip velocity magnitude distributions of silica sand–water and zircon sand–water slurry flows ($\rho_s = 2381$ kg/m^3, $\rho_z = 4223$ kg/m^3, $\rho_w = 988.2$ kg/m^3, $\alpha_k = 20\%$, $d = 0.0221$ m, $d_p = 0.00011$ m). (a) Slip velocity magnitudes along the horizontal centerline, (b) slip velocity magnitudes along the vertical centerline.

the central part of the pipeline, the slip velocity magnitude is kept in a small variant range. In the lower part, the slip velocity magnitude is dropped down sharply due to the larger slurry density and volume fraction of solids near the wall and non-slip boundary condition on the wall. On the other hand, the slip velocity magnitude would be increased, and the central part along the vertical centerline would be decreased, with an increase in the slurry density, as shown in Fig. 7(b). In any case, based on Fig. 7, it is clear that the effect of the slip velocity on the slurry flow is negligible in the heterogeneous and sliding bed flow (or moving bed flow) because the slip velocity magnitude is small.

5. Conclusions

The numerical investigation in slurry flows is valuable and interesting research because it can provide information that cannot be obtained in experiments. Based on our numerical investigations, the following conclusions can be made:

1. The ASM model can provide a good prediction for the liquid–solid slurry flow if the slurry mean velocity is higher than the corresponding critical deposition velocity. The numerical predictions for the pressure gradients are in good agreement with the experimental data.
2. The slurry density and volume fraction distributions are symmetric in the horizontal direction, but they would have a big gradient in the vertical direction. In heterogeneous and sliding bed flow (or moving bed flow), most of slurry flow on the top of the pipeline is water, while slurry mean density and volume fraction of solids would be increased gradually in the lower part of the pipeline. Slurry mean skin friction factor would be increased as the slurry mean velocity and solid particle density increase and would be constant in fully developed turbulent flow.
3. Velocity profiles in the slurry flow are symmetric in the horizontal direction, but they are asymmetric in the vertical direction. The velocity profiles in the upper part of the pipeline are higher than those in the lower part. The slip velocity magnitude is usually small, and the effect of the slip velocity on the slurry flow is negligible in the heterogeneous and sliding bed flow (or moving bed flow).

Acknowledgement

The authors gratefully acknowledge the financial support of the National Science Foundation (NSF) under Award no. CMS-0085645.

References

Brown, N.P., Heywood, N.I., 1991. Slurry Handling: Design of Solid–Liquid Systems. Elsevier Science Publishing Co., New York.

Dormaal, J., Raithby, G.D., 1984. Enhancement of the SIMPLE method for predicting incompressible flow problems. Journal of Numerical Heat Transfer 7, 147–158.

Doron, P., Barnea, D., 1996. Flow pattern maps for solid–liquid flow in pipes. International Journal of Multiphase Flow 22, 273–283.

Doron, P., Barnea, D., 1993. A three-layer model for solid–liquid flow in horizontal pipes. International Journal of Multiphase Flow 19, 1029–1043.

Doron, P., Granica, D., Barnea, D., 1987. Slurry flow in horizontal pipes-experimental and modeling. International Journal of Multiphase Flow 13, 535–547.

Fluent Inc., 1996. FLUENT 5: User's Guide, vols. 1–4.

Launder, B.E., Spalding, D.B., 1974. The numerical computation of turbulent flows. Computer Methods in Applied Mechanics and Engineering 3, 269–289.

Manninen, M., Taivassalo, V., Kallio, S., 1996. On the Mixture Model for Multiphase Flow, VIT Publications, Technical Research Center of Finland.

Nassehi, V., Khan, A.R., 1992. A numerical method for the determination of slip characteristics between the layers of a two-layer slurry flow. International Journal for Numerical Method in Fluids 14, 167–173.

Newitt, D.M., Richardson, J.F., Abbot, M., Turtle, R.B., 1955. Hydraulic conveying of solids in horizontal pipes. Transactions of the Institute of Chemical Engineers 33, 93–113.

Parzonka, W., Kenchington, J.M., Charles, M.E., 1981. Hydrotransport of solids in horizontal pipes: effects of solids concentration and particle size on the deposit velocity. Canadian Journal of Chemical Engineering 59, 291–296.

Roco, M.C., Shook, C.A., 1985. Turbulent flow of incompressible mixtures. Journal of Fluids Engineering 107, 224–231.

Skudarnov, P.V., Kang, H.J., Lin, C.X., Ebadian, M.A., Gibbons, P.W., Erian, F.F., Rinker, M., 2001. Experimental Investigation of Single- and Double-Species Slurry Transportation in a Horizontal Pipeline. Proc. ANS 9th International Topical Meeting on Robotics and Remote Systems, Seattle, WA.

Vocaldo, J.J., Charles, M.E., 1972. Prediction of pressure gradient for the horizontal turbulent flow of slurries. Proc. 2nd Int. Conf. on the Hydraulic Transport of Solids in Pipes, Coventry, England, Paper no. C1, pp. 1–12.

Wasp, E.J., Kenny, J.P., Gandhi, R.L., 1979. Solid–Liquid Flow: Slurry Pipeline Transportation. Gulf Publishing Co, Houston, TX.

Wilson, K.C., Pugh, F.J., 1988. Dispersive-force modeling of turbulent suspension in heterogeneous slurry flow. The Canadian Journal of Chemical Engineering 66, 721–727.